GEOPHYSICAL RESEARCH LETTERS, VOL. 33, L20101, doi:10.1029/2006GL026519, 2006

Effect of plasmaspheric drainage plumes on solar-wind/magnetosphere coupling

Joseph E. Borovsky[1] and Michael H. Denton[2,3]

Received 6 April 2006; revised 11 July 2006; accepted 17 July 2006; published 19 October 2006.

[1] Evidence is uncovered that plasmaspheric drainage plumes flowing into the dayside reconnection site mass load the reconnection rate and thereby reduce the coupling of the solar wind to the Earth's magnetosphere. Solar-wind/magnetosphere coupling is statistically analyzed with the 1963–2003 OMNI2 data set matched up with the AE, AU, and PCI geomagnetic indices. Times when plasmaspheric drainage plumes are flowing are discerned using multiple spacecraft with plasma detectors in geosynchronous orbit. It is found that for a given value of $-vB_z$ of the solar wind, the geomagnetic indices AE, AU, and PCI are statistically lower when plasmaspheric drainage plumes are present than when plumes are not present. This is taken as a measure of a weakened coupling of the solar wind to the Earth's magnetosphere caused by the plumes. An Addendum examines the effects of polar-cap saturation on the auroral electrojet index. **Citation:** Borovsky, J. E., and M. H. Denton (2006), Effect of plasmaspheric drainage plumes on solar-wind/magnetosphere coupling, *Geophys. Res. Lett.*, *33*, L20101, doi:10.1029/2006GL026519.

[2] Evidence is found that supports the notion that a high-density plume of cold plasma draining from the outer plasmasphere into the dayside reconnection site can reduce the coupling of the solar wind to the Earth's magnetosphere. This has implications for geomagnetic storms and it indicates that at times be a control of the dayside reconnection rate from the magnetospheric side of the site.

[3] Plasmaspheric drainage plumes occur when geomagnetic activity increases after an extended period of geomagnetic calm. *Borovsky and Steinberg* [2006a] speculated that plasmaspheric drainage plumes could mass load the dayside reconnection site, reducing the rate of reconnection between the solar-wind plasma (the magnetosheath) and the magnetospheric plasma. In a separate study [*Borovsky et al.*, 2006], two-dimensional compressible-MHD simulations confirm that adding high-density plasma to one side of an active neutral line indeed slows the rate of reconnection. For reconnection at the dayside magnetosphere, if the reconnection rate is reduced then the coupling of the solar wind to the magnetosphere under southward interplanetary magnetic fields should be reduced. This letter shows evidence for this reduction.

[1]Space Science and Applications, Los Alamos National Laboratory, Los Alamos, New Mexico, USA.
[2]Physics and Astronomy, University of Southampton, Southampton, UK.
[3]Now at Space Plasma Environment and Radio Science, Department of Communication Systems, University of Lancaster, Lancaster, UK.

0094-8276/06/2006GL026519$05.00

[4] Solar-wind/magnetosphere coupling is explored with the OMNI2 data set of 1-hour-average solar-wind measurements [*King and Papitashvili*, 2005] as given by *Borovsky and Funsten* [2003] and *Borovsky and Steinberg* [2006b]. Southward-IMF ($B_z < 0$, GSM) intervals are examined and the strength of the coupling is measured by the amplitude of various dayside-oriented geomagnetic indices (AE, AU, and PCI) as a function of $-vB_z$ of the solar wind. These geomagnetic indices are indications of the strength of auroral activity and are proportional to the amount of energy transferred to the Earth via solar-wind/magnetospheric coupling [cf. *Baumjohann*, 1986]. A 1-hour time lag is used on the geomagnetic indices AE and AU, but not on PCI; the time lags represent the approximate response time of the magnetosphere and improve the correlation coefficients between the solar wind and the indices [see *Borovsky and Funsten*, 2003; *Borovsky*, 2006].

[5] During prolonged intervals of geomagnetic quiet, the outer plasmasphere fills out to geosynchronous orbit and beyond [*Sojka and Wrenn*, 1985]. A subsequent increase in magnetospheric convection will strip away the outer plasmasphere and a plasmaspheric drainage plume will be formed [*Grebowsky*, 1970; *Spiro et al.*, 1981] wherein high-density plasma flows from the middle magnetosphere to the dayside reconnection site. The morphology of the plasmaspheric drainage plume is sketched in Figure 1. The cold plasma of the drainage plumes has been seen against the magnetopause [*Borovsky et al.*, 1997] and exiting the dayside neutral line [*Su et al.*, 2000, 2001]. For dayside reconnection between the magnetosheath and the magnetosphere, the drainage plume ($n \sim 10$'s cm^{-3}) represents a great increase in plasma density from the "empty" dayside magnetosphere ($n \sim 0.2$ cm^{-3}), greatly reducing the Alfven velocity of the magnetospheric plasma flowing into the dayside reconnection site. One naturally expects that Alfven speeds control the rate of reconnection [*Birn et al.*, 2001].

[6] For the coupling studies, one cannot discern with absolute certainty all of the times wherein plasmaspheric drainage plumes are ongoing in the outer magnetosphere. However, using multispacecraft observations of cold plasma in geosynchronous orbit a useful catalog of drainage-plume times can be produced. At geosynchronous orbit (dashed curve in Figure 1) these plumes are typically a few hours wide in local time on the dayside of the magnetosphere [*Elphic et al.*, 1996; *Weiss et al.*, 1997]. Times wherein plasmaspheric drainage plumes are ongoing are determined by spotting cold, dense plasmaspheric plasma near local noon at geosynchronous orbit using the multispacecraft MPA (Magnetospheric Plasma Analyzer) plasma detectors [*Bame et al.*, 1993]. In the years 1990–2003, whenever a geosynchronous spacecraft carrying an MPA detects cold plasma with a number density $n > 10$ cm^{-3} within ±2 hours

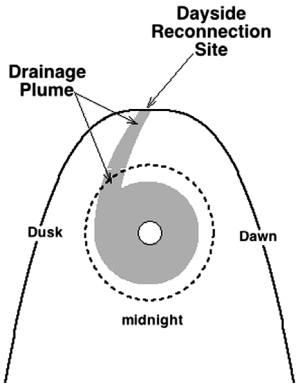

Figure 1. A view of the magnetosphere looking downward from above the Earth's north pole is sketched to show the morphology of a plasmaspheric drainage plume. The high-density cold plasma of the inner plasmasphere and the drainage plume is shaded in gray. The Earth is the white circle in the center. The magnetopause is the solid curve and the dashed circle is geosynchronous orbit (6.6 R_E). Note that the cold plasma of the plasmaphere $\mathbf{E} \times \mathbf{B}$ drifts, hence it flows where the magnetic-field lines flow, which is toward and into the dayside reconnection site. After Figure 5 of *Borovsky and Steinberg* [2006a].

of local noon, the time is denoted as a time of drainage-plume sighting. Any hour of UT in which there is at least one drainage-plume sighting is denoted as a "plume-on" hour. Note two things. (1) Owing to the limited number of MPA detectors in geosynchronous orbit, not all of the actual plume-on hours are found. (2) Some of the "plume-on" hours are actually times when the outer plasmasphere is very large and extends to beyond geosynchronous orbit on the dayside; as shown in the next paragraph, these times will be removed if we restrict our study to times of high Kp.

[7] In Figure 2 the number of "plume-on" hours is binned as a function of Kp (solid curve). In a similar fashion, the number of hours wherein cold plasma with a density of $n > 10$ cm^{-3} is sighted within ±2 hours of local midnight is also binned (dashed curve). Near local noon dense cold plasma is found at geosynchronous orbit under two conditions: (a) when there is a drainage plume or

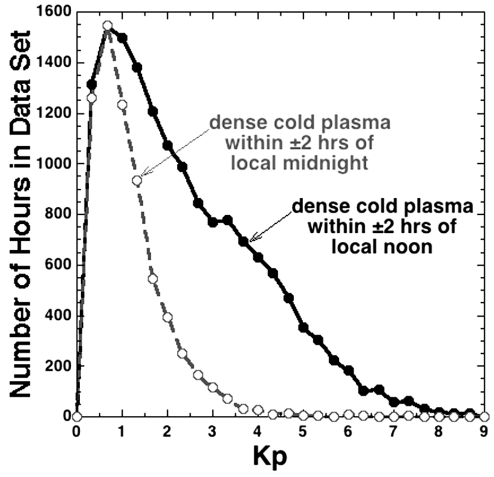

Figure 2. The number of hours of UT wherein MPA spacecraft detect $n > 10$ cm^{-3} in two ranges of local time is binned as a function of Kp, ±2 hours of local noon (solid curve) and ±2 hours of local midnight dashed curve. The height of the midnight distribution is multiplied by 1.21 to make the maximum values of the two distributions equal.

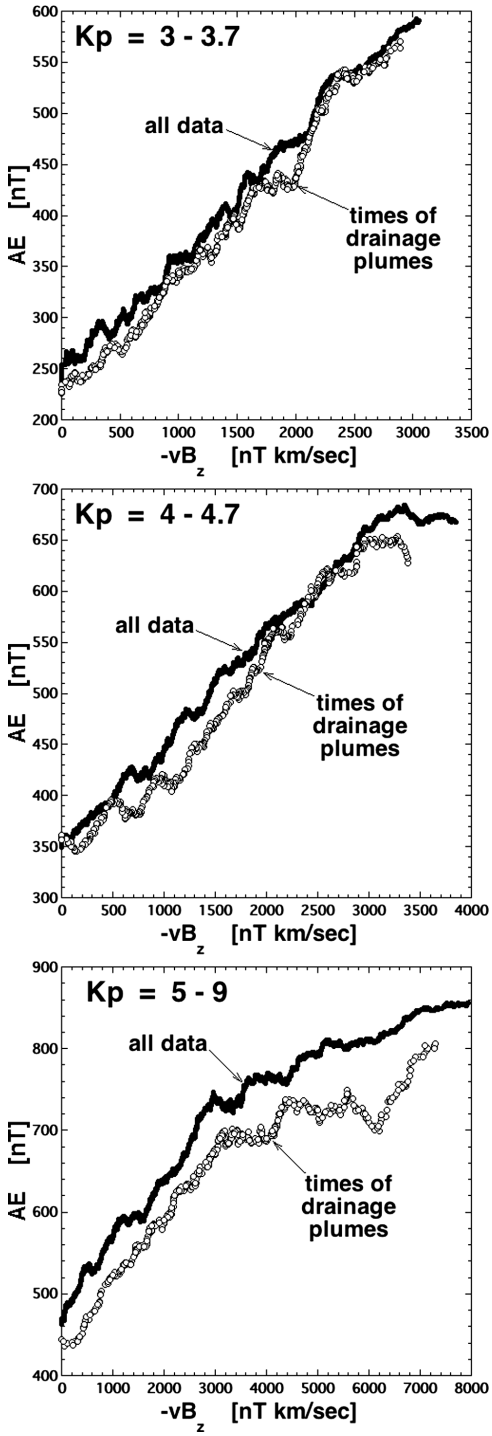

Figure 3. The one-hour-lagged auroral electrojet index AE is plotted as a function of $-vB_z$ (GSM) of the solar wind for three different ranges of Kp. The solid points are 600-point running averages of all of the OMNI2 data for 1963–2003 and the hollow points are 100-point running averages of the OMNI2 data during the plume-on times in 1990–2003.

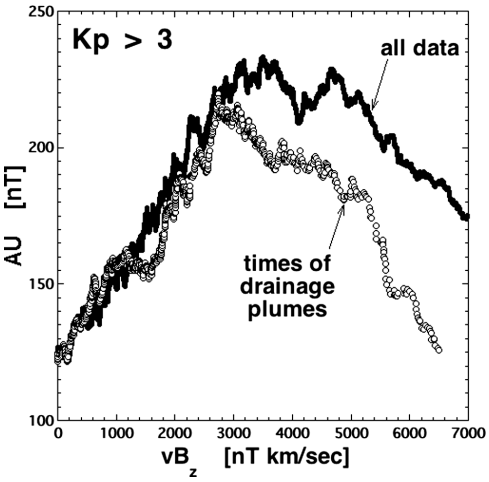

Figure 4. The one-hour-lagged auroral electrojet index AU is plotted as a function of $-vB_z$ (GSM) of the solar wind. The solid points are 600-point running averages of all of the 1963–2003 OMNI2 data for Kp > 3 and the hollow points are 150-point running averages of the OMNI2 data during the plume-on times in 1990–2003 while Kp > 3.

(b) when the outer plasmasphere is built up beyond geosynchronous orbit. Near local midnight dense cold plasma is found at geosynchronous orbit only under the condition that the outer plasmasphere is built up beyond geosynchronous orbit. The range of Kp values for which outer plasmasphere is found can be discerned from this nightside distribution. As can be seen in Figure 2, only for Kp less than about 3 will the outer-plasmasphere be seen. Hence, if we restrict our studies to intervals where Kp > 3, the "plume-on" hours will have little contamination from outer-plasmasphere intervals. For Kp > 3, about 14% of the time a drainage plume is ongoing according to the analysis of the MPA data set.

[8] To discern the effects of the drainage plumes, geomagnetic activity is plotted as a function of $-vB_z$ of the solar wind twice: once for all available data and once for only plume-on hours. Then the two are compared.

[9] In Figure 3 the AE index is plotted as a function of $-vB_z$ of the solar wind for three different ranges of Kp. The solid points are from all times and the hollow points are from "plume-on" times. The points plotted are running averages (boxcar averages) of the data to show the trends underlying a scatter of data points. The boxcar averages are 600-points wide for the "all times" and 100-points wide for the "plume-on" times. As Kp goes higher, there are fewer and fewer outer-plasmasphere times in the plume-on data set (see Figure 2). As can be seen in Figure 3, for a given value of $-vB_z$, the AE index is consistently lower during times when plasmaspheric drainage plumes are present in the magnetosphere than for general times. This indicates that solar-wind magnetosphere coupling is weaker for times when plasmaspheric drainage plumes are ongoing.

[10] In Figure 4 the AU index is plotted as a function of $-vB_z$ for Kp > 3, once for all data (solid points) and once for "plume-on" times (hollow points). Again the points plotted are running averages of the data. As can be seen, the AU index is lower for a given value of $-vB_z$ of the solar wind for the plume-on times than it is for ordinary times. This again supports the notion that solar-wind magnetosphere coupling is weaker for times when plasmaspheric drainage plumes are ongoing.

[11] In Figure 5, the polar-cap index (PCI Thule) [*Troshichev et al.*, 1988] is plotted as a function of $-vB_z$ for Kp > 3, once for all data (solid points) and once for "plume-on" times (hollow points). As can be seen, the polar cap index is lower for a given value of $-vB_z$ for the plume-on times than it is for ordinary times. This yet again supports the notion that solar-wind magnetosphere coupling is weaker for times when plasmaspheric drainage plumes are ongoing.

[12] Note that there are breakpoints in all-data and drainage-plume curves of Figures 3 and 4 which complicate their interpretation. As demonstrated in the Addendum, these breakpoints may be caused by polar-cap saturation during specific types of solar wind.

[13] For Kp > 3, the sizes of the decreases in the geomagnetic indices in Figures 3–5 are discerned by fitting curves to the points plotted and comparing the fits; the plume-produced decreases in the indices range from 1% to 11% for the auroral electrojet index AE, 2% to 43% for the auroral electrojet index AU, and 0% to 8% for the polar cap index PCI. In all cases larger fractional decreases occur when the $-vB_z$ driving is the strongest. It should be expected that there will be cases in which the decreases can be larger than these values since drainage plumes with relatively low densities ($n \sim 10$ cm^{-3}) were allowed into this study whereas plume densities as high as 100 cm^{-3} can be found [e.g., *Borovsky et al.*, 1997, Figure 4].

[14] The simple conclusion of this letter is that the solar-wind driving of the magnetosphere is weakened when plasmaspheric drainage plumes are occurring. We believe that this weakening is owed to a mass loading of the dayside reconnection site by the high-density cold plasma of the plume. The weakening is discernable but not overwhelming; it is on the order of a 10% effect.

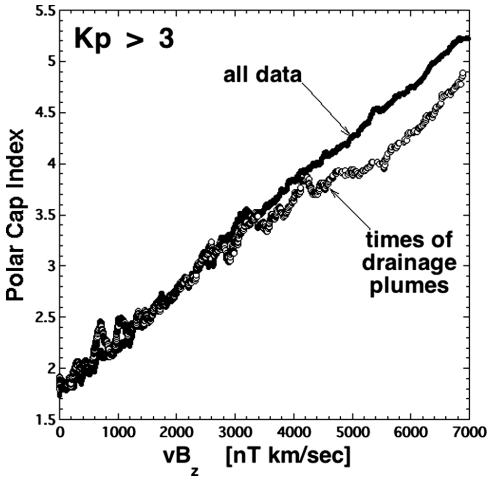

Figure 5. The polar cap index PCI (Thule) is plotted as a function of $-vB_z$ (GSM) of the solar wind. The solid points are 600-point running averages of all of the OMNI2 data in 1963–2003 for Kp > 3 and the hollow points are 150-point running averages of the OMNI2 data during the plume-on times in 1990–2003 while Kp > 3.

[15] Since strong drainage plumes occur after an extended interval of geomagnetic calm, one implication is that storms that are preceded by calms may differ from storms without calms. CIR driven storms tend to be preconditioned by lulls in geomagnetic activity more often than CME-driven storms are [*Borovsky and Denton*, 2006]. About 2/3 of all CIR-driven storms have calms preceding them and about 1/3 of CME-driven storms have calms [*Borovsky and Steinberg*, 2006a].

[16] Since the driving of the magnetosphere changes when plasmaspheric drainage plumes form, modelers studying the solar-wind-driven magnetosphere should consider adding a dense plasmasphere to their global 3-D MHD simulations to get the most-accurate results for storms and to see the fullest range of stormtime effects.

[17] To shore up and extend the conclusions of this letter, two studies are envisioned. (1) The magnitude of the decrease in solar-wind coupling should be quantified as a function of the number density of the observed drainage plumes in the dayside magnetosphere. (2) It is important to discern the actual rate of flux merging in the dayside reconnection site and to compare that merging rate for plume and no-plume cases.

[18] Motivated by the findings of this letter, three future studies are suggested. (1) Since the driving of the magnetosphere changes when plasmaspheric drainage plumes are present, and since the drainage plumes are more prominent after extended intervals of calm, geomagnetic storms with calms should be statistically compared with storms without calms to discern the range of differences that this change in driving produces. In such a study it is important to sort out these effects from the effects of cool dense plasma sheet which can increase the effectiveness of solar-wind/magnetospheric coupling for geomagnetic indices [*Lavraud et al.*, 2006]. (2) Since the reduction in driving is believed to be caused by a mass loading of the dayside reconnection site, the density of the magnetosheath may also be able to mass load the reconnection site, so one should consider statistically looking for a magnetosheath-Alfven-speed dependence to solar-wind/magnetosphere coupling. (3) For strong $-vB_z$ driving, there are break points to the geomagnetic-index-versus-vB_z curves of Figures 3–5; the analysis contained in the Addendum indicates that the breakpoints may be associated with polar-cap saturation. To better see the reduction in coupling by plumes the statistical data sets should be separately analyzed for polar-cap-saturation times and for non-saturation times.

Appendix A: Polar-Cap Saturation in the Measurements of Solar-Wind/Magnetosphere Coupling

[19] The *Siscoe et al.* [2004] theory of polar-cap saturation was examined from a solar-wind-driving point of view by *Borovsky and Denton* [2006] and it was pointed out that polar-cap saturation results when the unshocked solar wind has a high internal Alfven speed during times when the dayside ionospheric conductivity of the Earth is high. Specifically, polar-cap saturation occurs when the parameter $Q \equiv v_A S_N^{1/2}/1050 > 1$, where v_A is the Alfven speed in the solar wind (in km/s) and S_N is the sunspot number (which is a proxy for F10.7, which is a proxy for dayside ionospheric conductivity). According to Figures 10–12 of *Borovsky and Denton*, Q is high for CMEs (coronal mass ejections, including magnetic clouds) that occur during solar maximum. Using parameters in the OMNI2 data set, supplemented by the sunspot number, Q is calculated on an hourly resolution and the OMNI2 solar-wind data is sorted according to the value of Q. In Figure A1 solar-wind/magnetosphere coupling ($-vB_z$ to AE with a 1-hour lag on AE) is examined for three sortings of the data: no polar-cap saturation (blue points), polar-cap saturation (green points), and all data (black points). The points plotted are 200-point boxcar averages of the data sets. Comparing the curve of blue (unsaturated) points with the curve of green (saturated) points in Figure A1, one can see that the unsaturated-polar-cap AE-versus-vB_z relation (blue) remains linear at large values of $-vB_z$ whereas the polar-cap-saturated AE-versus-vB_z relation (green) has a breakpoint at $-vB_z \approx 2000$ nT km/s. (The $-vB_z$ position of this breakpoint depends on the range of Q values used.) Note that the green curve extends to larger values of $-vB_z$ than the blue curve does; this is because in the OMNI2 solar-wind data set the largest values of $-vB_z$ tend to be associated with CMEs at solar maximum, which tend to result in large Q values. The black curve in Figure A1 is for all data, unrestricted as to the value of Q. The black all-data curve displays a breakpoint at large $-vB_z$ as does the green curve. The interpretation of this breakpoint in the black

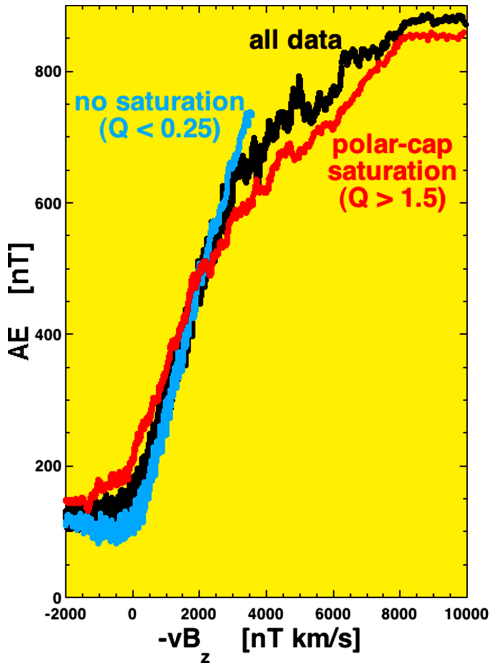

Figure A1. The one-hour-lagged auroral electrojet index AE is plotted as a function of $-vBz$ (GSM) of the solar wind. The black data points are for all data in the 1963–2003 OMNI2 data set, the blue data points are for strictly unsaturated polar cap ($Q < 0.25$) in the 1963–2003 data set, and the green data points are for saturated polar cap ($Q > 1.5$) in the 1963–2003 data set. In each case 200-point running averages are displayed and no restrictions on the values of Kp are used.

curve is that at very large $-vB_z$ the 1963–2003 OMNI2 data set is dominated by polar-cap-saturation solar wind (i.e., CMEs at solar maxima), which has an AE-versus-vB_z curve that has a breakpoint. Hence, in the solar-wind/magnetosphere coupling studies of this letter the breakpoints observed in the various plots may be owed to the dominance of polar-cap-saturation in the data sets for the large $-vB_z$ data points.

[20] The physical reason why AE is reduced for polar-cap saturation is not addressed in this addendum and should be the subject of a future study.

[21] **Acknowledgments.** The authors wish to thank the UK Solar System Data Centre at Rutherford Appleton Laboratory. J.E.B. wishes to thank the University of Southampton for their hospitality. This work was supported by the NSF National Space Weather Program and by the US Department of Energy.

References

Bame, S. J., D. J. McComas, M. F. Thomsen, B. L. Barraclough, R. C. Elphic, J. P. Glore, J. T. Gosling, J. C. Chavez, E. P. Evans, and F. J. Wymer (1993), Magnetospheric plasma analyzer for spacecraft with constrained resources, *Rev. Sci. Instrum.*, *64*, 1026.

Baumjohann, W. (1986), Merits and limitations of the use of geomagnetic indices in solar-wind-magnetosphere coupling studies, in *Solar Wind-Magnetosphere Coupling*, edited by Y. Kamide and J. A. Slavin, p. 3, Terra Sci., Tokyo.

Birn, J., et al. (2001), Geospace Environmental Modeling (GEM) magnetic reconnection challenge, *J. Geophys. Res.*, *106*, 3715–3720.

Borovsky, J. E. (2006), The eddy viscosity and flow properties of the solar wind: CIRs, CME sheaths, and solar-wind/magnetosphere coupling, *Phys. Plasmas*, *13*, 056505.

Borovsky, J. E., and H. O. Funsten (2003), Role of solar wind turbulence in the coupling of the solar wind to the Earth's magnetosphere, *J. Geophys. Res.*, *108*(A6), 1246, doi:10.1029/2002JA009601.

Borovsky, J. E., and M. H. Denton (2006), Differences between CME-driven storms and CIR-driven storms, *J. Geophys. Res.*, *111*, A07S08, doi:10.1029/2005JA011447.

Borovsky, J. E., and J. T. Steinberg (2006a), The "calm before the storm" in CIR/magnetosphere interactions: Occurrence statistics, solar wind statistics, and magnetospheric preconditioning, *J. Geophys. Res.*, *111*, A07S10, doi:10.1029/2005JA011397.

Borovsky, J. E., and J. T. Steinberg (2006b), The freestream turbulence effect in solar-wind/magnetosphere coupling: Analysis through the solar cycle and for various types of solar wind, in *Recurrent Magnetic Storms: Corotating Solar Wind Streams*, *Geophys. Monogr. Ser.*, vol. 167, edited by B. T. Tsurutani et al., AGU, Washington, D. C.

Borovsky, J. E., M. F. Thomsen, and D. J. McComas (1997), The superdense plasma sheet: Plasmaspheric origin, solar wind origin, or ionospheric origin?, *J. Geophys. Res.*, *102*, 22,089–22,106.

Borovsky, J. E., M. H. Denton, and M. Hesse (2006), What does the plasmasphere do to the magnetosphere?, *Eos Trans. AGU*, *87*(36), Jt. Assem. Suppl., Abstract SM53A-02.

Elphic, R. C., L. A. Weiss, M. F. Thomsen, D. J. McComas, and M. B. Moldwin (1996), Evolution of plasmaspheric ions at geosynchronous orbit during times of high geomagnetic activity, *Geophys. Res. Lett.*, *23*, 2189–2192.

Grebowsky, J. M. (1970), Model study of plasmapause motion, *J. Geophys. Res.*, *75*, 4329–4333.

King, J. H., and N. E. Papitashvili (2005), Solar wind spatial scales in and comparisons of hourly Wind and ACE plasma and magnetic field data, *J. Geophys. Res.*, *110*, A02104, doi:10.1029/2004JA010649.

Lavraud, B., M. F. Thomsen, J. E. Borovsky, M. H. Denton, and T. I. Pulkkinen (2006), Magnetospheric preconditioning under northward IMF: Evidence from the study of CME- and CIR-driven storms, *J. Geophys. Res.*, *111*, A09208, doi:10.1029/2005JA011566.

Siscoe, G., J. Raeder, and A. J. Ridley (2004), Transpolar potential saturation models compared, *J. Geophys. Res.*, *109*, A09203, doi:10.1029/2003JA010318.

Sojka, J. J., and G. L. Wrenn (1985), Refilling of geosynchronous flux tubes as observed at the equator by GEOS 2, *J. Geophys. Res.*, *90*, 6379–6385.

Spiro, R. W., M. Harel, R. A. Wolf, and P. H. Reiff (1981), Quantitative simulation of a magnetospheric substorm. 3. Plasmaspheric electric fields and evolution of the plasmapause, *J. Geophys. Res.*, *86*, 2261–2272.

Su, Y., J. E. Borovsky, M. F. Thomsen, R. C. Elphic, and D. J. McComas (2000), Plasmaspheric material at the reconnecting magnetopause, *J. Geophys. Res.*, *105*, 7591–7600.

Su, Y., J. E. Borovsky, M. F. Thomsen, N. Dubouloz, M. O. Chandler, T. E. Moore, and M. Bouhram (2001), Plasmaspheric material on high-latitude open field lines, *J. Geophys. Res.*, *106*, 6085–6096.

Troshicev, O. A., V. G. Andrezen, S. Bennerstrom, and E. Friis-Christensen (1988), Magnetic activity in the polar cap—A new index, *Planet. Space Sci.*, *36*, 1095.

Weiss, L. A., R. L. Lambour, R. C. Elphic, and M. F. Thomsen (1997), Study of plasmaspheric evolution using geosynchronous observations and global modeling, *Geophys. Res. Lett.*, *24*, 599–602.

J. E. Borovsky, Space Science and Applications, LANL, Los Alamos, NM 87545, USA. (jborovsky@lanl.gov)

M. H. Denton, SPEARS, Department of Communication Systems, University of Lancaster, Lancaster LA1 4WA, UK.